

Heat transfer and mapping of THz radiation absorption in biological tissue using *Mathematica* based *Simulink* transform

Usman Malik*, Krisman, Riad Syech, Muhammad Hamdi

Medical Physics, Biophysics Computation and Instrumentation, Physics Department, Science Faculty, University of Riau Pekanbaru Riau, Indonesia

* Corresponding author: mhdhamdi13@gmail.com

Article history

Received 27 February 2018

Revised 28 Mac 2018

Accepted 21 May 2018

Published Online 16 December 2018

Abstract

This work is built on the *Mathematica-Simulink* transformed modeling which emphasizes on the rate of heat generation when occurs radiation absorption with low scattering in attenuation against tissue radial and axial depth. Experimental based data and prediction of thermal distribution owing to absorption has applied a closed-form system known in principle as an analogue computer model. There are assumptions which considered to modeling principle and sample conditions such as static tissue with no blood supply with response to homeostatic regulation of body temperature equilibrium. Thermal transfer of different power densities indicates that it penetrates the axial or radial depth with the small heat change difference for several types of tissue, i.e., skin, fat, tumor, and muscle. The results for time intervals of one second or longer show a steady-state centered about one temperature. By contrast, milliseconds to picoseconds time ranges display a small but significant temperature change as the depth varies correlated with the contrasting tissue structures. The dimensionless temperature used for finding indifference of tissue thermal characteristics that gives the heat mapping in different contours of the dimensionless temperature. This indicates that the THz regime has a good prospect for clinical purpose and medical therapy as well as imaging.

Keywords: Radiation, modeling, absorption, thermal mapping, biological tissue

© 2018 Penerbit UTM Press. All rights reserved

INTRODUCTION

Terahertz radiation is a part of the infrared region included microwave region of the electromagnetic spectrum. It has specific properties sensing to moisture medium. This research determines the THz radiation regime absorption owing to the interaction between THz radiation and homogeneous tissue. The main connection in the software of *Mathematica* programming is to connect with transforming multi dimensional transfer functions of *Matlab*. Here we discuss a system to apply link of the main software such as *Mathematica* and *Simulink* in *Matlab*. This system is a *Mathematica-Simulink* transformed the system from a model constructed by interconnecting the blocks of *Simulink*. It is based on modeling of THz radiation regime heat transfer through tissue. We calculate on the rate of heat generation when occurs radiation absorption with low scattering in attenuation against the tissue radial and axial depth. Analogue computer model principle is constructed for determination of temperature distribution through biological tissue which uses a closed-form thermal-change system due to THz continuous wave radiation regime absorption at room temperature [1-3]. There are assumptions to be considered to modeling principle and sample conditions of static and dynamic tissue. We use the different power of THz radiation heat transfer through tissues in which gives certain interpretations by a ratio of transmission and reflection intensity in the

abnormal-normal cell tissue layer. The design constitutes dynamics modeling with applying the *Mathematica-Simulink* transformed system. The computation of modeling uses numerical methods with a power source of THz radiation regime in the range of (0.1-1) THz while comparisons use the experiment results of other researcher and other numerical methods in a terahertz range close to lower far infrared for studying validation.

THz radiation heat transfer of different power densities indicates that there is the significant small change in the heat transfer against axial and radial depth for several types of tissue with the various time of milliseconds-picoseconds range [4-6]. The results for time intervals of one second or longer show a constant temperature or a steady state-centered about one temperature. By contrast, milliseconds to picoseconds time ranges display a small but significant temperature change as the depth varies from initial condition to a depth of about 0 °C. Types of tissue show various temperature distributions for a THz power source which result in different maximum tissue depth and time steps 1 ps with a small temperature change gradually approaching zero. It is clear to be correlated with the contrasting tissue structures. The computation of modeling for comparison with this system has used the numerical methods with a range of THz power density source in (10-150) mW.m³ and a frequency range of (0.1-1) THz. They show the same achievement results of thermal distribution temperature in the various time and boundary conditions. A good agreement is

observed which fat indicates higher in heat transfer than skin and muscle to refer on the difference of tissue characteristics.

METHODOLOGY OF MODELING

Model of blood-supplied tissue in THz radiation-tissue interaction

The increase of the blood perfusion rate by dilation of the blood vessels is near the heated area that induced to remove the heat by the convection effect and when the vessels are coagulated, the blood perfusion rate decreases. As illustrated in Fig.1, the replica tissue structure depicts the dynamics of THz radiation-tissue interaction with its processing is nonlinear. It is complex process which makes it extremely difficult to predict the final effect of THz radiation irradiation. The whole nonlinear dynamic process of THz radiation-tissue interaction is not discussed. In the case of bioheat transfer, the computational domain may be selected as a cylindrical form in the rectangular box. The computational domain can be considered in 1 D coordinate, using different coordinate systems.

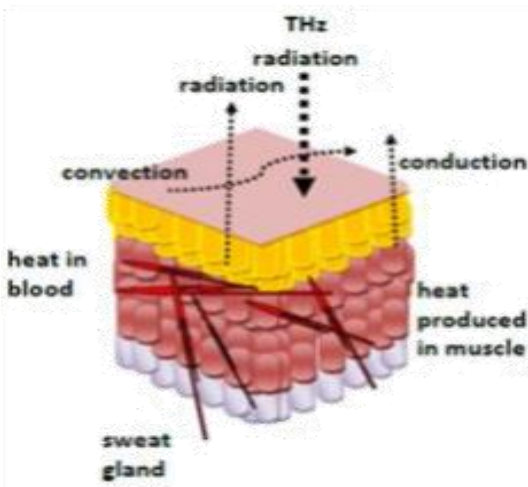


Fig. 1 A dynamic tissue model.

The numerical solution of the mathematical model provides a quantitative description of the heat reaction of bio-tissues when irradiated by the THz radiation source. Tissue optics is distinguished from conventional optics through its interest in the response of biological tissues to THz radiation regime. Biological tissue is nonhomogeneous, and in many cases, a tissue layer which absorbs and scatters the THz radiation energy based upon its optical properties. Absorbed photon energy is relaxed either non thermally or thermally.

Non thermally relaxed photons carry a different wavelength from the original wavelength (fluorescence) [7-9]. These photons are used for diagnosis. The most absorbed energy is relaxed thermally and causes the rise in tissue temperature. When the temperature rise and the time at that temperature progress above a certain threshold, then the tissue is thermally damaged and coagulated. This thermal damage process is determined by thermal damage parameters. In most cases, the temperature rise and corresponding thermal coagulation change the optical properties, thermal properties, and blood perfusion rate of biological tissues as discussed earlier. Following the coagulation, the light energy is redistributed based upon the new optical properties during THz radiation irradiation. The thermal properties such as thermal conductivity, density, and specific heat of tissue are functions of tissue water content. Since temperature rise causes evaporation of the water contents at the surface of the irradiated tissue, the thermal properties also change.

A mathematical model for the thermal field is Pennes equation of the bioheat and it describes the thermal behavior based on the classical Fourier's law [6, 9]. The model results of this theoretical analysis will enable to understand and answer the following statements:

1. The change on the temperature field of THz radiation behaviors with a heat release of terahertz radiation at THz frequencies and since water has strong absorptions [10-12] and cancer cell tissues tend to have different water content from normal tissue [13-19] when penetrating at boundaries of each tissue layer.
2. The effect on the penetration of terahertz radiation at interfaces of cancers-normal and other tissue layers appears the significant changes of heat release distribution [18-26] and owing to the existence of involving factors of absorption, reflection, refraction, dispersion and scattering [24-27].

The THz radiation source is assumed to be vertically incident upon the tissue surface and has power in 15 mW-150 mW and a beam radius of 2 mm. The total exposure time is minute-picoseconds, and the initial temperature is set at room temperature and body temperature at 37°C. In this study, the original data sources refer several references [25, 27, 7, 10, 28-30]. A result of the modified table can be seen in Table 1. The established numerical or analytical calculation of tissue optical and thermal properties as compared with the experimental data of FTIR and THz pulse. The THz radiation fluence rate calculated using the input parameters in Table 1. The verification for the temperature calculations using analogue computer technique is performed by a comparison with an analytic, numerical solution and others In Fig.1a depicts the block diagram of a body thermoregulatory dynamics model for analyzing the thermal transfer of terahertz radiation in tissue. It has a purpose of knowing absorption rate which is related to the THz radiation regime electric field. Theory of compartment for energy rate Q in biophysics it considers substances of tissue structure as an interesting analogy which explains into the partition concept of compartments. Meanwhile in Fig. 1a and 1b, it explains principles of pulse transmission and Fig. 2a, 2b,2c and 2d there are main compartments to have a function as integrators. These ports are places of termination process for heat flux input and output in skin, fat, tumor and muscle tissue which are caused by THz radiation absorption. The temperature increase during the exposure is due to the THz radiation regime absorption in tissues. Absorption of power is characterized by specific absorption rate, which is related to the THz radiation regime electric field. To employ clearly in this thesis relate to the aspects of analysis which explains the descriptive research.

Derivation of Modeling Equation

In Fig. 3, if a part of body response to increase heat to be used to control the heat rise process in tissue due to the penetration of THz radiation, then it needs the accurate information about the change of temperature in the response of input of THz radiation heat during absorption in tissue. The energy change or accumulation in transient condition can be expressed in the following equation [2].

$$\text{accumulation} = \rho V C \frac{\partial T}{\partial \tau} \quad (\text{Joule / ps}) \quad (1)$$

Where V is volume of tissue, density ρ , specific heat C and time t independent variable, or in term of absorbed power density in the volume of tissue. By the assumption of equal inlet and outlet heat flow rate, which the mass of tissue is constant. Since

$$\text{accumulation} = \text{input} - \text{output} \quad (2)$$

then it can be expressed in the following equation

$$\rho V C \frac{\partial T}{\partial \tau} = Q_{in} - Q_{out} + Q_{ext} \quad (3)$$

Theory of compartment in biophysics it considers substances of muscle cancer tissue structure as an analogy which explains into the partition concept of compartments. There are two main compartments to have a function as integrators. These ports are places of termination process for input and output of heat flux in cancer and normal tissue which caused by THz radiation absorption (SAR) and thermoregulation of blood supply and metabolism such as a cell, other tissue, fat, heamoglobin (HB), and intracellular. This expression of cancer tissue can be given by the following equation:

$$\rho_c C_c \frac{\partial T}{\partial t} = K_c \nabla^2 T - \omega_b \rho_b C_b (T - T_a) + Q_{mt+others} + SAR \quad (4) \quad \frac{\partial T}{\partial t} = \nabla^2 T + \sum_{i=1}^N K_i Q_i(E, H, x, T), t > 0, 0 < x < L \quad (19)$$

For the muscle tissue, it is given by

$$\rho_m C_m \frac{\partial T}{\partial t} = K_m \nabla^2 T - \omega_b \rho_b C_b (T - T_a) + Q_{mt+others} + SAR \quad (5)$$

Equation (4 and 5) can be used only if temperature distribution in the system or in a part of the system is uniform, and the temperature is independent of spatial coordinates, $T(z,t) = T(t)$. This assumption of the uniform temperature distribution also implies that the system physical properties, such as density and specific heat, are constant within the system boundaries [2, 3, 5, 6, 9-12, 16].

$$SAR = \frac{2\mu_t \sigma E^2 T}{\pi \rho \delta w^2} \exp(-2r^2/w^2) \exp(-\mu_t z/\delta) \text{ (mW/kg)} \quad (6)$$

Where σ (S/mm) is the electric conductivity of tissue, ρ is the mass density in kg/m, $\mu = \mu_a + \mu_s$ (mm^{-1}) is the total attenuation coefficient absorption and scattering coefficient, w (mm) is a spot THz beam waist radius, δ (mm) is the penetration depth of THz radiation, r [47] is the distance from the power source, T is the fraction of transmitted power, and E is the root mean square (RMS) of THz radiation regime electric field strength in V/mm. If there is no response of body tissue, the relation between SAR, duration of exposure dt , and heat conduction due to change in temperature dT . These expressions of skin, fat, tumor and muscle tissue can be given by the following equations with involving constants of heat transport rate K ,

$$\frac{\partial T_s}{\partial t} = \nabla^2 T_s + \sum_{i=1}^N K_i Q_i + SAR, t > 0, 0 < x < L \quad (7)$$

$$\frac{\partial T_f}{\partial t} = \nabla^2 T_f + \sum_{i=1}^N K_i Q_i + AR, t > 0, 0 < x < L \quad (8)$$

$$\frac{\partial T_t}{\partial t} = \nabla^2 T_t + \sum_{i=1}^N K_i Q_i + SAR, t > 0, 0 < x < L \quad (9)$$

$$\frac{\partial T_m}{\partial t} = \nabla^2 T_m + \sum_{i=1}^N K_i Q_i + SAR, t > 0, 0 < x < L \quad (10)$$

Equation (7-10) can be used only if temperature distribution in the system or in a part of the system is uniform, and the temperature is independent of spatial coordinates, $T(z,t) = T(t)$. This assumption of the uniformity temperature distribution also implies that the system physical properties, such as density and specific heat, are constant within the system boundaries. For the specific reason involving pointing vector power hence $S = E \times H$ and terahertz power source Q (E, H, T, x) into the physical magnetic and electric field intensity Maxwell's equations are set in the time domain is the most natural approach. It starts with solving the following main Maxwell's equations together with the heat conduction equation simultaneously subjected to the following initial and boundary conditions,

$$\frac{\partial E}{\partial t} = \nabla^2 E + \sum_{i=1}^N K_i Q_i(E, H, x, T), t > 0, 0 < x < L \quad (11)$$

$$\frac{E_{i+1,j} - E_{i,j}}{k} = \frac{-E_{i+2,j} + 16E_{i+1,j} - 30E_{i,j} + 16E_{i-1,j} - E_{i-2,j} + \sum_{i=1}^N K_i Q_i(E, H, x, T)}{12h_i^2} \quad (12)$$

$$E(x, 0) = (1 - rf)E(x, 0) \quad (13)$$

$$E(L, t) = (1 - rf)E(L, t), \{0 < t, 0 < x < L\} \quad (14)$$

$$\frac{\partial H}{\partial t} = \nabla^2 H + \sum_{i=1}^N K_i Q_i(E, H, x, T), t > 0, 0 < x < L \quad (15)$$

$$\frac{H_{i+1,j} - H_{i,j}}{k} = \frac{-H_{i+2,j} + 16H_{i+1,j} - 30H_{i,j} + 16H_{i-1,j} - H_{i-2,j} + \sum_{i=1}^N K_i Q_i(E, H, x, T)}{12h_i^2} \quad (16)$$

$$H(x, 0) = (1 - rf)H(x, 0) \quad (17)$$

$$H(L, t) = (1 - rf)H(L, t), \{0 < t, 0 < x < L\} \quad (18)$$

$$\frac{T_{i+1,j} - T_{i,j}}{k} = \frac{-T_{i+2,j} + 16T_{i+1,j} - 30T_{i,j} + 16T_{i-1,j} - T_{i-2,j} + \sum_{i=1}^N K_i Q_i(E, H, x, T)}{12h_i^2} \quad (20)$$

$$T(x, 0) = (1 - rf)T(x, 0) \quad (21)$$

$$T(L, t) = (1 - rf)T(L, t), \{0 < t, 0 < x < L\} \quad (22)$$

Where $Q(E, H, x, T)$ is the THz power heat source, density ρ , electric conductivity σ and permittivity ϵ . Fields arise from currents and charges on the source. The analogue computer differential analyzer is really a transient analyzer, in that conditions at the beginning of the interval of integration must be fed into the machine and the final results are taken as they come. If conditions at both ends of an interval of integration are specified, in general not enough is known about the starting conditions so that upon integration the correct final conditions will result. This means that the trial solution must be made for assumed starting conditions and then by interpolation or extrapolation the correct starting conditions determined to satisfy the required final conditions. It is imagined that equations [7-10] have some physical quantities in which solution of temperature T depends on parameters from K_1, K_2 to K_i which are derived from experimental data. The parameters K_1, K_2 and up to K_i typically carry some uncertainties resulting from the experiment that is used to measure them. We attempt to calculate the resulting uncertainty in the quantity T by using the total derivative of the expression. Assume that parameters K_1, K_2 up to K_i carry uncertainties, $dT(K_1), dT(K_2)$, and up to $dT(K_i)$, respectively, but the parameter K_i is a well known constant without any significant uncertainty. Assuming that linear approximations are adequate, the uncertainty in the derived quantity T is then can be determined.

The Mathematica-Simulink transformed program building

The Mathematica-Simulink transformed program building environment for biophysics and the medical application has been developing in which the computer imaging and signal processing software mathematica is as transformer software from modelling of Matlab-Simulink based dynamic systems. It can be seen in Fig. 2. It is applied for the analysis of Simulink-based dynamic systems with models constructed through the analogue circuit step in Fig. 3 using equation 7, 8, 9 and 10. Simulink designs are transformed to Mathematica through Matca-Smlink Programs under the control of a modified Mathematica graphical user interface. The applications in imaging and signal processing of simulink dynamics modelling are described in which block-transformed nonlinear systems coded in Matca-Smlink Programs passed to Mathematica. Mathematica is employed to determine the transfer functions that connecting the system outputs to the system inputs and this system is applied to obtain the timely responses and the harmonic responses of the system.

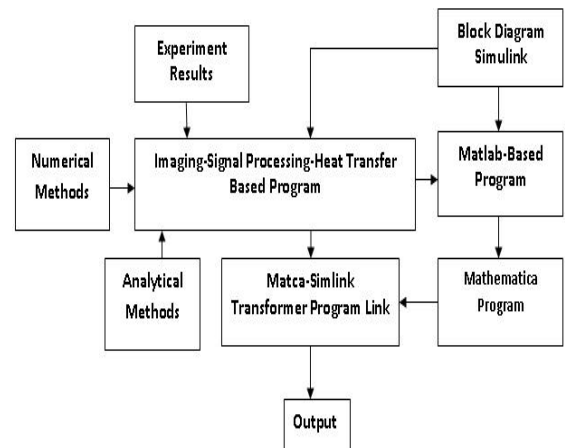


Fig. 2 Graphical transformer environment of Mathematica-Simulink system based software building linkages.

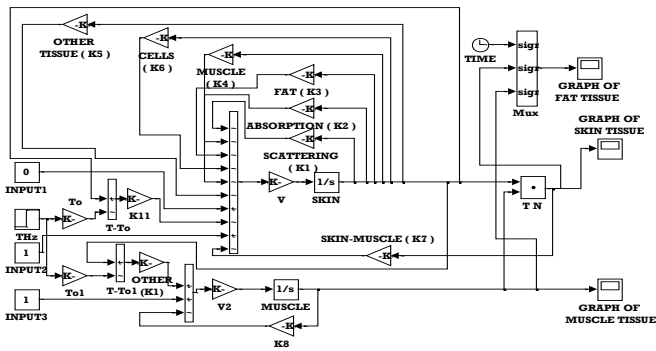


Fig. 3 Block diagram of THz heat transfer through biological tissue using Simulink-based Matlab system.

Table 1 Thermal, electric, optical properties and parameters of the biological medium [19-31].

Kinds of Parameters	Value	Unit	Unit
Specific Heat Capacity	3950	j/kg °c	
Tissue Density	1055	kg/m ³	
Thermal Conductivity	0.642	w/m °c	
Heat Convection Coefficient	10	w/m °c	
Blood Specific Heat Capacity	4180	j/kg °c	
Blood Specific Heat	4200	j/kg °c	
Blood Density	1000	kg/m ³	
Blood Perfusion Rate	40	cm/s	
Blood Average	0.45	cm/s	
Permeability	1	a/m	
Dielectric Constant	5		
Electric Conductivity	0.3	s/m	
Absorption Coefficient	9.75	cm ⁻¹	
Propagation Coefficient	12.16	cm ⁻¹	
Refraction Index	2.1 ± 0.4	np/m	
Metabolism Heat Generation	33800	kg/m ³ s	

RESULTS AND DISCUSSION

THz radiation heat conduction in milliseconds-picoseconds range

In the analysis of the heat transfer through tissue involving the heat conduction equation, there arises a scale of sort time concerned with the relaxing time. It focuses on solutions in response to pulse absorption of THz radiation. The Fig.4 show that temperature distribution is instantaneous to propagate at every point in tissue from incident pulse which arises effect. During this duration, the temperature fluctuates in a range of millisecond-picoseconds. This effect indicates that in fast time and a short distance in which case of THz radiation pulse could travel lesser than the light speed. This means that the initial cause problem exists on the fact which THz radiation pulse gives a response to the excitation of molecules. This response tends to form a step which needs time for the reestablished equilibrium known as the time of relaxation. Determination of this condition depends on the process of microscopic collision. The natural time scale of the physical problem which marks out the domain of validity of the Fourier law is thus the relaxation time [28, 29, 32-41, 52]. Results of analytical calculation have been employed to analyze and predict about biological tissue 1 D THz radiation heat conduction for the thermal transient state of temperature small change in millisecond-picoseconds time biological tissue 1 D THz radiation heat conduction for the thermal transient state of temperature small change in the millisecond-picoseconds time range. With using THz picoseconds time range, based on theoretically derived analytical solutions.

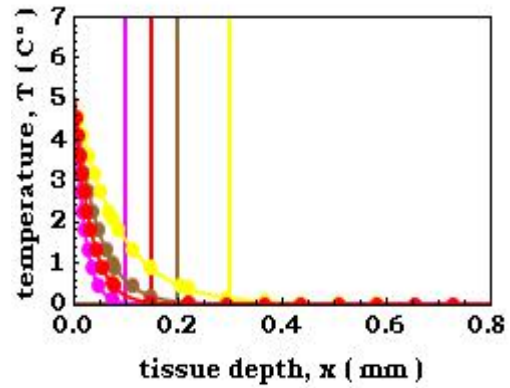


Fig. 4 Analysis of 1 D heat conduction for the thermal transient state.

Analyses focus on particularly in relaxation times of pulse propagation. The results for time intervals of one second or longer show a constant temperature or a steady state-centered about one temperature. By contrast, millisecond to picosecond time ranges display a small but significant temperature change as the depth varies from x=0 mm to a depth at which T=0 °C. In Fig. 4 they show the use of time intervals for several types of tissue in skin (brown), fat (yellow), tumor (pink), or muscle (red) to obtain temperature distributions as functions of tissue depth. Skin tissue shows heat conduction with maximum tissue depth 0.2 mm and time steps 10⁻¹²s or 1 ps with a small temperature change gradually approaching zero. It is thinner than fat tissue 0.3 mm but thicker than tumor 0.1 mm or muscle tissue 0.15 mm, correlated with the contrasting tissue structures [42-46,52].

Analysis of dimensionless parameters

In this research we discuss the dimensional analysis of thermal distribution constitutes an expression in parameters of dimensionless temperature concerning a ratio of the same unit. THz radiation heat transfer in kinds of tissue yield a number of pertinent dimensionless groups that are, in general, analogous to dimensionless groups for depth of tissue. Calculation computes the heat transfer in cancer tissue which results in the thermal distribution using two different axis depth conditions such as radial and axial axis direction. In Fig. 5a and b they show two different heat distributions. Axial depth describes that ratio of temperature dimensionless concerning heat transfer of THz radiation absorption decreases more sharply than that of radial depth axis. It means that when THz radiation is absorbed in cancer tissue then the resulting heat in the axial axis direction propagates faster and larger than that of the radial axis direction. In principle, the important analysis of dimensionless parameter aims as the determination of medium characteristic heat transfer number factor. It is a medium properties group analogous like bio medium, plasma, gas, fluid and solid.

The thermal distribution shows that the generation of heat connected to the THz radiation regime absorption strength in Fig. 5. THz radiation heat transfer of three different tissues with a power 50 mW indicates that the dimensionless temperature to depth in various tissues such as skin [30-35], fat (blue) and muscle (red) tissue varying for the exposure in 1 ps with THz radiation beam waist radius 5 mm, fraction of transmitted power 1. Basically, It is necessary to be found accurately numerical data for certain ranges of transmitted and reflected energy to the biological tissues at Terahertz frequencies.

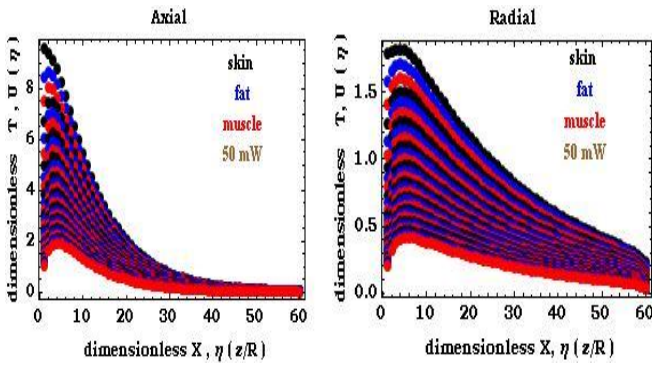


Fig. 5 Analysis of dimensionless temperature for temperature change (a) Axial and (b) Radial Depth

Temperature distribution using mathematica-simulink transformed system and comparisons

A result of the graphs in Fig. 6, application of the *Mathematica-Simulink* transformed system or analogue computer method (ACM) it is iterated in time until an asymptotic temperature profile is achieved. To compare the predicted and empirically measured temperature, the results are saved at predetermined intervals. The thermal distribution experiment measurement with exposure of terahertz radiation various powers on each kind of normal tissue surface and inside abnormal tissue bodies are considered. In Fig. 6a and 6b as comparison studies of the thermal structure of tissue layers such as skin, fat, and muscle for exploring deeply the smallest temperature change against the depth of each tissue layer with the use of different frequency 0.1 THz and 1 THz and power 100 mW and 150 mW, respectively.

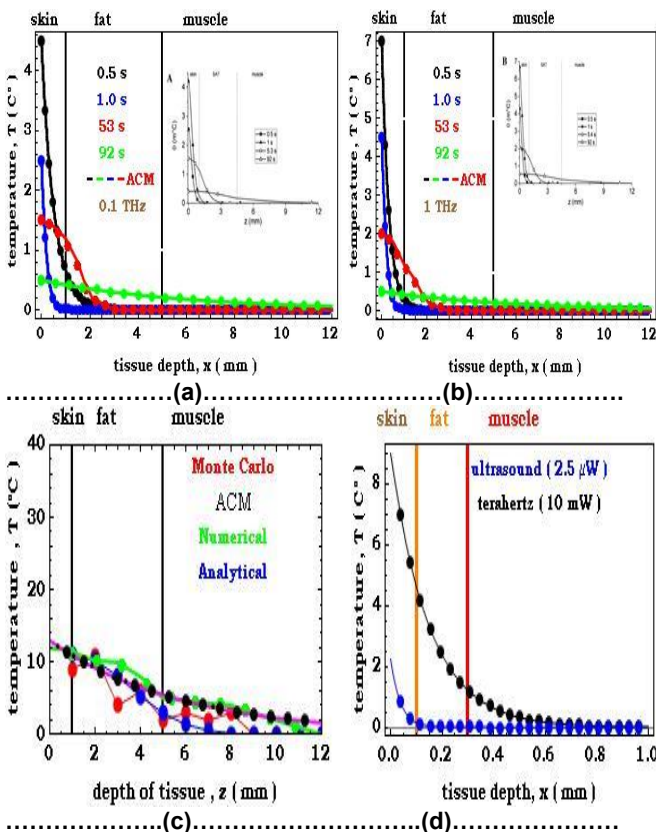


Fig. 6 Temperature small change through a structure of tissue layers with (a) 0.1 THz and (b) 1 THz (c) Comparison in other methods and (d) Ultrasound and Terahertz.

They show temperature distribution results for absorption through tissue structure. An analogue computer method is compared with other methods such as *Monte Carlo*, analytical, and numerical method. It seems most of the same attainment. Meanwhile in Fig. 6b and 6c, both ACM and experiment data describe the same approach

results. The thermal distributions of ACM and experiment data (in the graph) shows that the heat generated is directly related to using of the 0.1 and 1 THz. For use of different power sources between ultrasound and terahertz, there is a significant difference in temperature distribution of both them. Terahertz has absorption strength higher than ultrasound which can be seen in Fig. 6d. In Fig. 6a and 6b show heat transfer of two different frequencies indicate significant results in the heat changes against the depth of tissues for the exposure in time $t = 0.5, 1.5, 3$ and 92 . Therefore the present investigation is more capable of dealing with many practical bioheat transfer problems than some other suggested analytical solutions. The low frequency of 0.1 THz can result in temperature changes such as T about 0.5, 1.5, 2.5, and 4.5 °C with increasing tissue depth and vice-versa. Whereas using of frequency 1 THz irradiates in several time durations resulting in T about 0.5, 2, 4.5, and 7.0 °C. When power with these frequencies penetrates the depth of tissue then their loss of powers reach zero about 12 mm. It is obvious to show the significant temperature decrease of each power density sharply. The high (red) and medium (blue) power density results in a high-temperature change against the depth of tissues; whereas the low power density [21, 23, 30, 31] shows the slight temperature change to remain constant gradually.

These reasons indicate that heat mechanisms are principally connected with the THz radiation regime absorption depending on tissue dielectric complex property and thermal parameters. In a structured modeling of three tissue layers we use solving the fundamental heat conduction equation which has empowers with different frequency. It can be seen that there is a significant change in temperature when the use of different frequency irradiates in the time period. The time required for these temperatures to return to near base levels, which is critical for determining THz radiation signal repetition rate, is considerably longer than the theoretically-defined thermal relaxation time. Physically, it is obvious to understand that two identical quasi-conductor media (e.g. fat and muscle tissue cell) with the same boundary conditions may evolve differently if they start with the same initial temperatures. This interpretation with the focused model solutions depends on the bioheat conduction main parameters such as a tissue cell heat conduction attenuation, THz radiation heat conduction wave, and thermal diffusivity. To better understand the heat conduction in muscle cancer tissue physical interpretation using the heat conduction equation; it needs to look more in detail on the thermal properties of normal muscle tissue. For physical problems, it is not sufficient to know that the problem exists and has a unique solution. Hence the continuity requirement is not only useful but also essential.

VISUALIZATION OF THZ RADIATION HEAT MAPPING IN TISSUE

Mapping of tissue heat conduction

In quantum optics, the visualization of causal interpretation for energy density plot is observed through the trace of THz radiation photon in tissue using Monte Carlo method. It can be seen in Figure in Fig. 7a. Dark shading color agrees with the room temperature about 25 °C. Consider heat transfer given by heat conduction equation which represents heat conduction mapping in a two-dimensional domain. The 2D technique is applied for visualizing in area depicting and using the amplitude mapping of the 2D color map as can be seen in Fig. 7a. The area in x and y coordinate is in where at an origin point as a beginning position of radiation source trace that travels randomly in tissue to form a trajectory going randomly from down to up, the THz radiation position in the direction of x -axis from left to right, and the radial distance r from a diagonal direction toward top. It seems to fluctuate with the small vibrations of radiation trace toward the top in a radial direction. Interpretation of this performance can be analyzed structurally by an amplitude of waveforms. The other visualization to interpret this data is emphasizing on observables of energy density or the flux density which transforms into real space. This displays the qualities and quantities synchronically as shown in Fig. 7a. As a vectorial quantity with arrows from the energy flux density can be visualized most intuitively. In Fig.7b, 7c and 7d the boundary conditions are such that the temperature on all the edges of the domain

equal to 0. Without loss of generality, one can take the thermal diffusivity of skin, fat and muscle is α equal to 0.05 cm²/s, 0.07 and 0.003, respectively. The initial condition is given in room temperature. The dimensionless temperature can be found using the Chebyshev collocation technique. As shown in Fig. 7a, 7b, and 7c they give the results in different contours of the dimensionless temperature. They are shown using the various colors for the high temperature in red and low temperature in orange. Perfect agreement is observed which fat indicates higher in heat transfer than skin and muscle. It refers on the difference of tissue characteristics. The purpose of this heat mapping is to visualize the relationship between heat transfer rate and wavelength that varies thermal conductivity of tissue kinds by applying scattering factor. This visualization plots the heat production rate versus wavelength through the depth of tissue. It investigates a modified bio-heat model. The equation, which includes the calculation of factors that affect the heat production rate per unit volume in cell tissue. This analysis uses various tissues with a power source of 100 mW. Fat shows high heat production rate (red) among skin and muscle. THz radiation penetrates biological tissue by analyzing the scattering, which depends on the angle and wavelength.

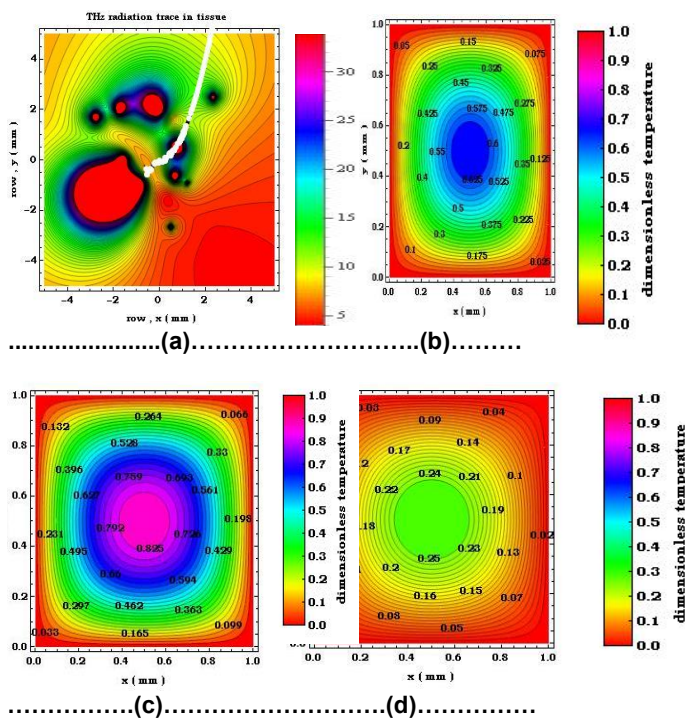


Fig. 7(a) Causal interpretation visualization in energy density, contours of heat conduction mapping in (b) Skin, (c) Fat, (d) Muscle.

The Instantaneous power density through tissue

A qualitative interpreting of the THz radiation pulse penetration into tissue performs the illustration of visualization way in an area with passing sequences of pulse propagation through tissue cell slits. The different stages of THz radiation absorption into tissue in the frequency region of (0.1–1), they indicate understanding the dosimetric significance from the THz radiation exposure to tissue. The calculation of THz radiation energy into heat energy inside a tissue small volume is computed with using the energy per unit time. Application of the contour technique interprets the instantaneous power density in arbitrary units or decibels. In Fig. 8, it describes causal interpretation visualization in energy density contour plot for THz radiation absorption behaviors in two different tissues fat (left) and muscle (right). In Fig. 8a, 8b, and 8c they show the transformation of energy flows from source to medium which the radiation energy comes from absorption in fat ($n = 1.35$, left) near a small interface slab of fat-muscle ($n = 1.38$, right). They depict that how the influence of the fat-muscle interface thickness is having the size about THz radiation wavelength. In Fig. 8 a if radiation has the same wavelength or close to the interface thickness with a layer width $d = 1.9 \mu\text{m}$ and a

factor of regularity $\Delta=0.2$ then the radiation energy in such systems does not go from the fat to muscle directly, but from the fat to its intersection point at or inside the layer interface. This means that it reaches a stage of energy equilibrium at the boundary. It can be analogous to refer to the fields' combination of two-oriented radiation dipoles with regularity factor. One of both is the source of radiation energy while the second dipole is a sink of tissue cell energy. In Fig. 14 b energy flows when the wavelength of the radiation dipole is less from the interface thickness with layer width $d = 2.5 \mu\text{m}$ and a factor of regularity $\Delta=0.5$.

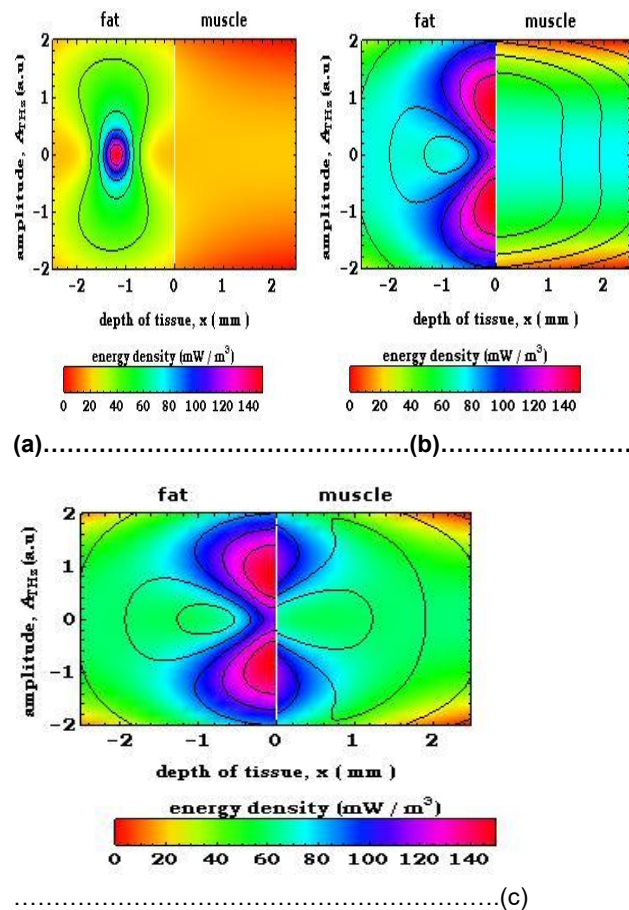


Fig. 8 Causal interpretation visualization in energy density contour for regularities (a) 0.2, (b) 0.5 and (c) 0.7.

Fig. 8c THz radiation source in fat flows to penetrate an interface of fat-muscle with a layer width $d = 2.5 \mu\text{m}$ and a factor of regularity $\Delta=0.7$. Biological tissue is a complex and highly heterogeneous material, especially in a microscopic scale with typical dimensions comparable to the wavelength of visible light. Scattering arises from the microscopic variations and inhomogeneities of the refractive index which correspond to various scattering centers in tissue, while the reciprocal is referred to as the mapping in the interference pattern. It shows the low scattering mean free path. In imaging of quantum optics the probability distribution of THz radiation photons absorption passing through two tissue cell slits, which produces heat in the quantum-optical probability distribution for a photon of THz radiation scattered by a model of a cylindrical tissue cell, starting from Gaussian THz waveform state. Interference phenomena are exhibited as the number of time steps is increased. To solve this Schrödinger equation, the analysis uses the finite-difference method, incrementing the time variable in steps of Δt . This section presents a theoretical framework which calculates the energy density of the THz radiation regime in Fig. 9 with the diffusing-heat wave absorption for low scattering case as introduced in recent theoretical work. A dipole far field of THz radiation absorbs surface of the tissue which propagates with 0.1 THz and 1 THz frequency through diameters of two cell slits. Fig. 9a and 9b show the existence of which propagates with 0.1 THz

and 1 THz frequency through diameters of two cells slit. Fig. 9a, 9b, 9c, and 9d as well as 9e, 9f show the existence of absorption coefficient against variable of THz frequency for tumor and fat cell tissue. In fact, each tissue describes that a range of low THz frequencies about 1 THz there is a significant thermal rise of absorption and while it indicates a low heat rise of about 0.1 THz. Also, it shows its absorption strongly for fat cell tissue but muscle cell tissue absorbs weakly. Consideration of tissue is as a discrete ensemble of scatterers. The dominant scatterers in a tissue may be the fibers, cells, or subcellular organelles. The probability density that a photon incident on a small volume element will survive is equal to the ratio of the scattering and extinction cross sections and is called the "albedo" for single scattering. The albedo ranges from zero for a completely absorbing medium to unity for a completely scattering medium.

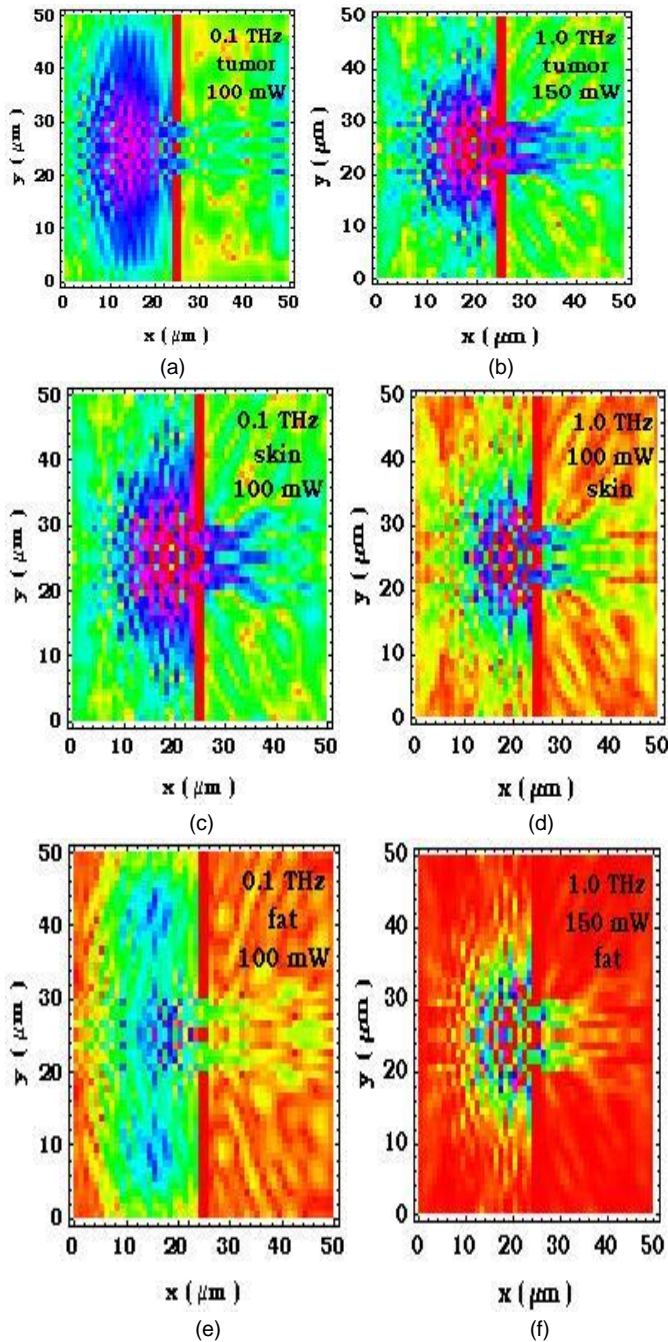


Fig. 9 Visualization of instantaneous power density (a) and (b) tumor (c) and (d) skin and (e) and (f) fat.

In Fig. 10 there are on the short cell diameter scales as a slit which the propagation becomes increasingly ballistics in two slits of different tissue cell. It refers to the low scattering of various THz radiation

frequencies capable of describing the crossover from ballistic to diffusive propagation. It shows that the polarization dependence of the auto-correlation function for a diameter of the cell size. Low scattering spectroscopy implies on the fact that dielectric fluctuation is sufficiently weak that the THz radiation scattered by the entire tissue medium. The following assumptions are made in this model which the frequency of the scattering radiation remains exactly the same as that of the incident radiation. Therefore, the scattering process is elastic. Phenomena of THz radiation absorption in muscle cancer tissue describe the fraction of the radiation after attenuation by absorption and scattering, provided that this penetrates the tissue. This result can help to better understand the temperature history of cancer cell tissues subject to step heating and thus suggest requirements for the cancer-killing temperatures.

The rate of THz heat production with low scattering

The Fig. 10a shows that the change from a shorter to a longer wavelength increases the heat production rate in a cancer cell volume slightly (measured in mW/mm²). This means that shorter wavelengths contribute to the heat production more than the longer wavelengths. It also indicates that the longer wavelengths remain constant. In Fig.10b shows that in with various power densities due to penetration of THz photon radiation variation about d = 20mm reduces temperature change to zero and also due to properties of tissue optical depth, δ = 1 mm. Other factors include the variation of the THz radiation power sources and the variation of the wavelengths, as well as the radiation photon incidence angles. Because the higher heat production is caused by the THz radiation regime beam for 0.1 THz and 1 THz propagating through the tissue with strong water absorption, the intensity is attenuated exponentially, due to the low scattering factor.

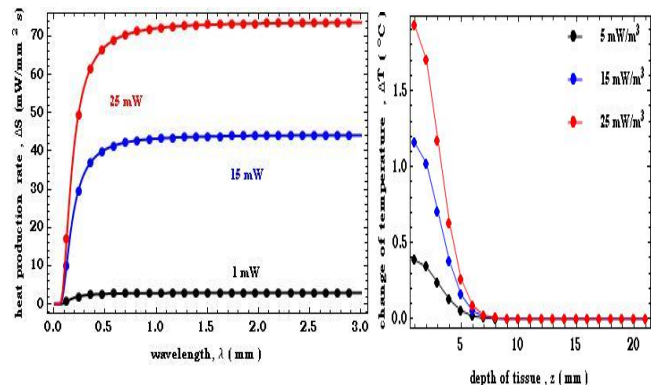


Fig. 10 Increase of temperature (a) Wavelength and (b) Depth of tissue for various power densities.

CONCLUSION

The results for time intervals of one second or longer show a constant temperature or a steady state centered about one temperature. By contrast, millisecond to picoseconds time ranges display a small but significant temperature change as the depth varies for each tissue such as skin, fat, tumour, or muscle from a certain depth correlated with the contrasting tissue structures. Numerical calculation for scattering effect computes the thermal distribution using two different depth conditions for thermal mapping such as radial and axial axis direction which it results in significant different cold-red thermal color distribution. Axial depth describes that ratio of temperature dimensionless concerning heat transfer of THz radiation absorption decreases more sharply than that of radial depth axis. It means that when THz radiation is absorbed in tissue then the resulting heat in the axial axis direction propagates faster than that of the radial axis direction. In principle the important analysis of dimensionless parameter aims for the determination of medium characteristics recognized as the heat transfer number factor. The modeling result of temperature distribution in biological tissue applies the *Mathematica-Simulink* based transformer or analogue computer method which compared with other numerical methods performing for all is almost

the same result approach. The parameters obtained between model and experiment data are quite accurate with the uncertainty or a propagation error is 0.8 %.

ACKNOWLEDGEMENT

The authors thank Medical Physics, Biophysics Computation and Instrumentation, Physics Department, Science Faculty, University of Riau Pekanbaru Riau, Indonesia for supporting the project.

REFERENCES

- [1] Yoshida, A., Kagata, K., Yamada, T. 2010. Measurement of thermal effusivity of human skin using the photoacoustic method. *International Journal of Thermophysics*, 31(10), 2019-2029.
- [2] Irene B. V. M., David A. M., Eric R. B. 2009. *Energy Transfer Systems Dynamics in Biomaterial*. Berlin: Springer-Verlag, p.256.
- [3] Modest, M. F. 2003. *Radiation Heat Transfer, Second Edition*. USA: Elsevier Science, p.105.
- [4] Alfano, R. R. 2005. *The Supercontinuum Laser Source: Fundamentals with Updated References* [2nd ed.].Springer, p257.
- [5] Yoshida, Z. 2010. *Nonlinear Science: The Challenge of Complex Systems*. First Edition. Berlin: Springer-Verlag, p.56.
- [6] Yang, D.2007. *Mossbauer Effect in Lattice Dynamics: Experimental Techniques and Applications*. First Edition. Wiley-VCH, p.426.
- [7] Angeluts, A. A., Balakin, A. V., Evdokimov, M. G., Esaulkov, M. N., Nazarov, M. M., Ozheredov, I. A., Sapozhnikov, D. A., Solyankin, P. M., Cherkasova, O. P., Shkurinov, A. P. 2014. Characteristic responses of biological and nanoscale systems in the terahertz frequency range. *Quantum Electronics*, 44(7), 614-632.
- [8] Hua, C., Shi-Hua, M., Wen-Xing, Y., Xiu- Mei, W., Xiao-Zhou, W. 2013. The diagnosis of human liver cancer by using THz fiber-scanning near-field imaging. *Chinese Physics Letters*, 30(3), 3070-3012.
- [9] Luca, I. Z., Arduino, A., Bottauscio, O., Chiampi, M. 2014. Parametric analysis of transient skin heating induced by Terahertz radiation. *Bioelectromagnetics*, 35(5), 314-323.
- [10] Kim, E. 2004. *Phthalocyanine Nanostructures*. World Scientific Publishing Company, p.62.
- [11] Z. Wang. 2001. *Physics with Maple: Computer Algebra for Mathematical Methods in physics*. First Edition. Wiley-VCH, p.610.
- [12] Hoppe, W. Lohmann, W., Markl, H., Ziegler. H. 1983. *Biophysics (First ed.)*. New York: Springer-Verlag, p. 276.
- [13] Ashley, J. Welch, Martin, J. C., Van Gemert. 2011. *Optical-Thermal Response of Laser-Irradiated Tissue (First ed.)*. England: Springer, p. 259.
- [14] Lopez-Molina, J. A., Rivera, M. J., Trujillo, M., Burdío, F., Lequerica, J. L., Hornero, F., Berjano, E. J. 2008. Assessment of hyperbolic heat transfer equation in theoretical modeling for radiofrequency heating techniques. *Biomedical Engineering Journal*, 2, 22-27.
- [15] Waigh, T. A. 2007. *Applied Biophysics a Molecular Approach for physical Scientists (First ed.)*. England: Copyright. John Wiley & Sons Ltd., p1022.
- [16] Pickwell, E., Cole, B. E., Fitzgerald, A. J., Pepper, M., Wallace, V. P. 2014. In vivo study of human skin using pulsed terahertz radiation. *Physics in Medicine and Biology*, 49(9), 1595-607.
- [17] Quarrie, D. A. M. 1983. *Quantum Chemistry (first ed.)*. England: Oxford University Press, p 209.
- [18] Lee, Y.-S. 2009. *Principles of Terahertz Science and Technology (First ed.)*. England: Springer Science + Business Media, LLC, p.246.
- [19] Barton, J. K., Gossage, K. W., Xu, W., Ranger-Moore, J. R., Saboda, K., Brooks, C. A., Duckett, L. D., Salasche, S. J., Warneke, J. A., Alberts, D. S. 2003. Investigating sun-damaged skin and actinic keratosis with optical coherence tomography: A pilot study. *Technology in Cancer Research and Treatment*, 2(6), 525-535.
- [20] Berry, E., Walker, G. C., Fitzgerald, A. J., Zinov'ev, N. N., Chamberlain, M., Smye, S. W., Miles, R. E., Smith, M. A. 2012. Do in vivo terahertz imaging systems comply with safety guidelines. *Journal of Laser Applications*, 15(3), 191-198.
- [21] Bruehlmeier, M., Roelcke, U., Blauenstein, P., Missimer, J., Schubiger, P. A., Locher, J. T., Pellikka, R., Ametamey, S. M. 2003. Measurement of the extracellular space in brain tumors using ⁷⁶Br-bromide and PET. *Journal of Nuclear Medicine*, 44(8), 1210-1218.
- [22] Caspers, P. J., Lucassen, G. W., Bruining, H. A., Puppels, G. J. 2010. Automated depth-scanning confocal raman microspectrometer for rapid in vivo determination of water concentration profiles in human skin. *Journal of Raman Spectroscopy*, 31, 813-818.
- [23] Cole, B., E., Woodward, R. M., Crawley, D. A., Wallace, V. P., Arnone, D. D., Pepper, M. 2001. Terahertz imaging, spectroscopy of human skin in vivo. *Proceedings of the SPIE*, 4276, 1-10.
- [24] Fitzgerald, A. J., Berry, E., Zinov'ev, N. N., Homer-Vanniasinkam, S., Miles, R. E., Chamberlain, J. M., Smith, M. A. 2003. Catalogue of human tissue optical properties at terahertz frequencies. *Journal of Biological Physics*, 129(2-3), 123-128.
- [25] Han, P. Y., Cho, G. C., Zhang, X.-C. 2013. Time-domain transillumination of biological tissues with terahertz pulses. *Optics Letters*, 25(4), 242-244.
- [26] Hou, D., Li, X., Cai, J., Ma, Y., Kang, X., Huang, P., Zhang, G. 2014. Terahertz spectroscopic investigation of human gastric normal and tumor tissues. *Physics in Medicine & Biology*, 59(18), 5423-5440.
- [27] Jafarieh, H. Yea. 2007. *Technology transfer to developing countries: A quantitative approach*. University of Salford, p.567.
- [28] Johnson, J. L., Dorney, T. D., Mittleman, D. M.2001. Interferometric imaging with terahertz pulses. *IEEE Journal of Selected Topics in Quantum Electronics*, 7(4), 592-599.
- [29] Kim, A. D. 2004. Transport theory for light propagation in biological tissue. *Journal of the Optical Society of America A*, 21(5), 820-827.
- [30] Klarskov, P., Clark, S. J., Jepsen, P. U. 2014. *Modeling of ultrafast THz interactions in molecular crystals. Proceedings Volume 8984, Ultrafast Phenomena and Nanophotonics XVIII; 89840D*. San Francisco, California, United States, p.1033.
- [31] Kleine-Ostmann, T., Jastrow, C., Baaske, K., Heinen, B., Schwerdtfeger, M., Kärst, U., Hintzsche, H., Stopper, H., Koch, M., Schrader, T. 2014. Field exposure and dosimetry in the THz frequency range. *IEEE Transactions on Terahertz Science and Technology*, 4(1), 21-25.
- [32] Knobloch, P., Schildknecht, C., Kleine-Ostmann, T., Koch, M., Hoffmann, S., Hofmann, M., Rehberg, E., Sperling, M., Donhuijsen, K., Hein, G., Pierz, K. 2002. Medical THz imaging: An investigation of histo- pathological samples. *Physics in Medicine and Biology*, 47(21), 3875-3884.
- [33] Löffler, T., Siebert, K., Czasch, S., Bauer, T., Roskos, G. 2002. Visualization and classification in biomedical terahertz pulsed imaging. *Physics in Medicine & Biology*, 47(21), 3847-3852.
- [34] Matti Hotokka, E. J. B., Gerardo, J. M., -Barrio, D. 2013. *Advances in quantum methods and applications in chemistry, physics, and biology. Volume 27 Molecular Theory of Graphene*. Springer-Verlag, p. 249-284.
- [35] Movasaghi, Z., Rehman, S., Rehman, I. U. 2008. Fourier transform infrared FTIR spectroscopy of biological tissues. *Applied Spectroscopy Reviews*, 43(2), 134-179.
- [36] Oh, S. J., Kim, S.-H., Jeong, K., Park, Y., Huh, Y.-M., Son, J.-H., Suh, J.-S. 2013. Measurement depth enhancement in terahertz imaging of biological tissues. *IEEE Transactions on Terahertz Science and Technology*, 21(18), 212-215.
- [37] Parrott, E. P., Sy, S. M., Blu, T., Wallace, V. P., Pickwell-Mac Pherson, E. 2011. Terahertz pulsed imaging in vivo: Measurements and processing methods. *Journal of Biomedical Optics*, 16(10), 106-110.
- [38] Peter, B. S., Yngvesson, S., Siqueira, P., Kelly, P., Khan, A., Glick, S., Karellas, A. 2013. Development and testing of a single frequency terahertz imaging system for breast cancer detection. *IEEE Transactions on Terahertz Science and Technology*, 3(4), 374-386.
- [39] Reid, C. B., Reese, G., Gibson, A. P., Wallace, V. P. 2013. Terahertz time-domain spectroscopy of human blood. *IEEE Journal of Biomedical and Health Informatics*, 17(4), 774-778.
- [40] Sakami, M., Mitra, K. M., Hsu, P.-F. 2012. Analysis of light pulse transport through two-dimensional scattering and absorbing media. *Journal of Quantitative Spectroscopy and Radiative Transfer*, 73(2-5), 169-179.
- [41] Saviz, M., Spathmann, O., Streckert, J., Hansen, V., Clemens, M., Dana, R. F. 2013. Theoretical estimations of safety thresholds for terahertz exposure of surface tissues. *IEEE Transactions on Terahertz Science and Technology*, 3(5), 635-640.
- [42] Scherer, P. O. J., Fischer, S. F. 2010. *Theoretical Molecular Biophysics (First ed.)*. Berlin: Springer-Verlag, p. 456.
- [43] Shiraga, K., Ogawa, Y., Suzuki, T., Kondo, N., Irisawa, A., Imamura, M. 2014. Characterization of dielectric responses of human cancer cells in the terahertz region. *Journal of Infrared, Millimeter, and Terahertz Waves*, 35(5), 493-502.
- [44] Sonka, M., Hlavac, V., R. Boyle, R. 1999. *Image Processing, Analysis and Machine Vision (Second ed.)*. Paci Grove: Brooks/Cole Publishing Company, p.379.
- [45] Wang, Z., S. M. I. 2001. Generation of terahertz radiation via nonlinear optical methods. *IEEE Transactions on Geosciences and Remote Sensing*, 1(1), 1-5.
- [46] Xu, M., Alfano, R. R. 2005. Fractal mechanisms of light scattering in biological tissue and cells. *Optics Letters*, 30(22), 3051-3053.

- [47] Xue, P., Mak, C., Cheung, H. 2014. New static lightshelf system design of clerestory windows for Hong kong. *Building and Environment*, 72, 368-376.
- [48] Yang, D., Converse, M. C., Mahvi, D. M., Webster, J. G. 2007. Expanding the bioheat equation to include tissue internal water evaporation during heating. *IEEE Transactions on Biomedical Engineering*, 54(8), 1382 - 1388.
- [49] Yue, K., Zhang, X., Yu, F. 2007. Simultaneous estimation of thermal properties of living tissue using noninvasive method. *International Journal of Thermophysics*, 28(5), 1470-1489.
- [50] Zaytsev, K. I., Kudrin, K. G., Koroleva, S. A., Fokina, I. N., Volodarskaya, S. I., Novitskaya, E. V., Perov, A. N., Karasik, V. E., Yurchenko, S. O. 2014. Medical diagnostics using terahertz pulsed spectroscopy. *Journal of Physics*, 486, 012-014.
- [51] Kindt, J. T., Schmuttenmaer, C. A. 1996. Far infrared dielectric properties of polar liquids probed by femtosecond terahertz pulse spectroscopy. *Journal of Physical Chemistry*, 100(24), 10373-10379.
- [52] Zhang, X. -C. 2002. Terahertz wave imaging: Horizons and hurdles. *Physics in Medicine and Biology*, 47, 3667-3677.